SCIENTIFIC REPORTS

OPEN

SUBJECT AREAS:
FERROELECTRICS AND MULTIFERROICS
CONDENSED-MATTER PHYSICS
ELECTRONIC DEVICES
SURFACES, INTERFACES AND THIN FILMS

Received
5 October 2012

Accepted
12 October 2012

Published
7 December 2012

Correspondence and requests for materials should be addressed to J.-H.C. (choijh@kist.re.kr) or C.S.H. (cheolsh@snu.ac.kr)

Strain evolution of each type of grains in poly-crystalline (Ba,Sr)TiO_3 thin films grown by sputtering

Woo Young Park[1], Min Hyuk Park[1], Jong Ho Lee[1], Jung Ho Yoon[1], Jeong Hwan Han[1], Jung-Hae Choi[2] & Cheol Seong Hwang[1]

[1]WCU hybrid materials program, Department of Materials Science and Engineering, and Inter-university Semiconductor Research Center, Seoul National University, Seoul 151-744, Korea, [2]Electronic Materials Research Center, Korea Institute of Science and Technology, Seoul 136-791, Korea.

The strain states of [111]-, [110]-, and [002]-oriented grains in poly-crystalline sputtered (Ba,Sr)TiO_3 thin films on highly [111]-oriented Pt electrode/Si substrates were carefully examined by X-ray diffraction techniques. Remarkably, [002]-oriented grains respond more while [110]- and [111]-oriented grains do less than the theoretically estimated responses, which is understandable from the arrangement of the TiO_6 octahedra with respect to the stress direction. Furthermore, such mechanical responses are completely independent of the degree of crystallization and film thickness. The transition growth temperature between the positive and negative strains was also different depending on the grain orientation. The unstrained lattice parameter for each type of grain was different suggesting that the oxygen vacancy concentration for each type of grain is different, too. The results reveal that polycrystalline (Ba,Sr)TiO_3 thin films are not an aggregation of differently oriented grains which simply follow the mechanical behavior of single crystal with different orientations.

The mechanical properties of materials are one of the fundamental material parameters, which are generally represented by the relationship between the strain (ε) and stress (σ). Sometimes, the ε and σ influence other fundamental properties of the materials, such as the electrical properties (piezoelectric effect) and defect distribution (piezochemical effect), as well as the mechanical response of the materials. Perovskite structured materials are a typical example showing such a correlation between the different fundamental properties due to their high ionic polarizability. Many perovskite oxide thin films, such as (Ba,Sr)TiO_3 (BST), showed a crucial influence of the ε and accompanying σ on the functionality of the films, such as the dielectric constant, polarization, Curie temperature, and piezoelectric coefficient[1–10]. The strain can even transform the non-ferroelectric phase to the ferroelectric phase and vice versa[11]. Recent theoretical calculations indicated that the strain also provides an important contribution to the dielectric and ferroelectric properties of the perovskite oxide/metal interfaces, which mostly govern the functionality of the nano-meter scale thin films[12–14].

The strain in thin films is induced by various intrinsic factors, such as the misfit strain and the thermal expansion mismatch with the substrate, as well as extrinsic factors, such as the impurity/vacancy incorporation and shot-peening effect in sputtering[15]. In many cases, many of these factors simultaneously influence the strain state of the perovskite oxide films, which renders the fundamental understanding on the influence of these factors on the properties of the films complicated and often disagree with the theoretical expectations.

The recent development in the fabrication techniques for the epitaxial perovskite oxide thin films[16–20] has greatly improved the experimental verification for the influence of the strain. However, the epitaxial systems often have limited usefulness regarding their use in many important applications, such as random access memory devices and integrated electro-mechanical systems, which are usually formed on Si substrate for commercial reasons. Si is very vulnerable to the chemical reaction and poorly lattice-matched with these perovskite oxides. Its thermal expansion mismatch is also non-favorable for improving the functionality. Due to these non-desirable factors of Si substrate, it is usually passivated with amorphous SiO_2 films and a poly-crystalline bottom electrode, typically Pt, which inevitably results in poly-crystalline perovskite thin films.

It must be quite a natural consequence that the strain state of the poly-crystalline film has a much more complicated pattern due to the non-uniform structure and crystallographic direction of each grain. It appears that there are two fundamental questions regarding the strain status of poly-crystalline films; what is the strain state of

each grain, and is the strain state of each grain influenced by the strain state of neighboring grains? The other question is what is the defect (typically oxygen vacancy) concentration in each grain and does this have a certain relationship with the strain state of each grain? These questions are difficult to answer even when using the state-of-the-art spectroscopic tools having high spatial resolutions since the defect concentrations are generally very low.

In this report, the authors attempted to answer these two important questions by adopting the X-ray diffraction (XRD) technique to the poly-crystalline BST thin films with a thickness of 120 nm which were deposited on highly [111]-orientation preferred poly-crystalline Pt thin film electrodes by an rf magnetron sputtering technique at substrate temperatures (T_s) ranging from 338 to 505°C. The different T_s results in the different stress state of the films; low and high T_s induced the overall in-plane compressive and tensile stresses, respectively, due to the dominance of the shot peening effect (at low T_s) and the mismatch in the thermal expansion coefficients of Si substrate and BST film (at high T_s). In addition, BST films with thicknesses ranging from 29.6 to 155.8 nm were deposited at 505°C in order to understand the influence of the film thickness on the stress and defect states of each grain. The strain state of each grain with different orientations was estimated by a careful XRD analysis using the $\sin^2\psi$ method. The results are compared with the expected strain-stress relationship from the bulk compliance values. Semi-quantitative discussions on the reason for the evolution of different stress-strain states based on the crystal structure of the perovskite material are presented.

Results

First, the influences of T_s on the structural properties of BST films are discussed. Experimental details and detailed information on the accurate thickness and cation compositions of each BST film are shown in the methods section and in *on-line supplementary information* (table SI), respectively. The films are usually slightly Ti-rich (Ti/(Ba+Sr+Ti) ~ 0.52) and Ba-deficient (Ba/(Ba+Sr) ~ 0.48). XRD spectra in Θ-2Θ mode of the BST films showed relatively random growth directions with (110), (111) and (002) peaks. Although the diffraction peak intensity generally increases with the increasing T_s, suggesting better crystalline quality and less mosaicity, the relative peak intensity ratio did not vary significantly. (See Fig. S1 of *on-line supplementary information*) The peak position generally shifts into the high 2Θ direction with the increasing T_s, suggesting that the films undergo more in-plane tensile stress due to the thermal expansion mismatch between the BST (~ 10 x 10^{-6} °C^{-1})[21] and the Si substrate (~ 2.62 x 10^{-6} °C^{-1})[22] while cooling down after the film deposition. Detailed strain evolutions for each type of grain in the different films were examined by the $\sin^2\psi$ method. Here ψ is the angle between the direction normal to the film surface and the direction of the specific crystallographic orientation where the inter-planar spacing was measured (ex, (112), (110), and (−112) planes for the [111]-oriented grains). Details for the $\sin^2\psi$ method can be found from Ref. 23 and its principle can be represented by Eq. (1) shown below.

Figures 1a-d show the variations in the lattice parameters of the Pt electrode film, [111]-, [110]-, and [002]-oriented BST grains, respectively, as a function of $\sin^2\psi$ for the BST films grown at different T_s. The data points were best linear fitted (lines) according to the Eq. (1);

$$\sqrt{h^2+k^2+l^2}\,d^{\psi} = \sqrt{h^2+k^2+l^2}\,d_0^{\psi}(\varepsilon_0-\varepsilon_z)\sin^2\psi + \sqrt{h^2+k^2+l^2}\,d_0^{\psi}(\varepsilon_z+1)a^{\psi} = a_0^{\psi}(\varepsilon_0-\varepsilon_z)\sin^2\psi + a_0^{\psi}(\varepsilon_z+1) \quad (1)$$

where, h, k, l, d^{ψ}, d_0^{ψ}, ε_{ψ}, ε_0, and ε_z are the three Miller indices, measured inter-planar spacing at the measurement angle ψ, and the calculated out-of-plane inter-planar spacing (ψ = 0), strain along the measurement direction ψ, in-plane strain, and out-of-plane strain, respectively. a^{ψ} and a_0^{ψ} are measured lattice parameters at the measurement angle ψ, and the calculated out-of-plane lattice parameter (ψ = 0). The positive and negative slopes correspond to in-plane tensile ($\sigma_0 > 0$, i. e. $\varepsilon_o > \varepsilon_z$) and compressive ($\sigma_0 < 0$, i. e. $\varepsilon_o < \varepsilon_z$) stress states, respectively. From the extrapolation of the linear

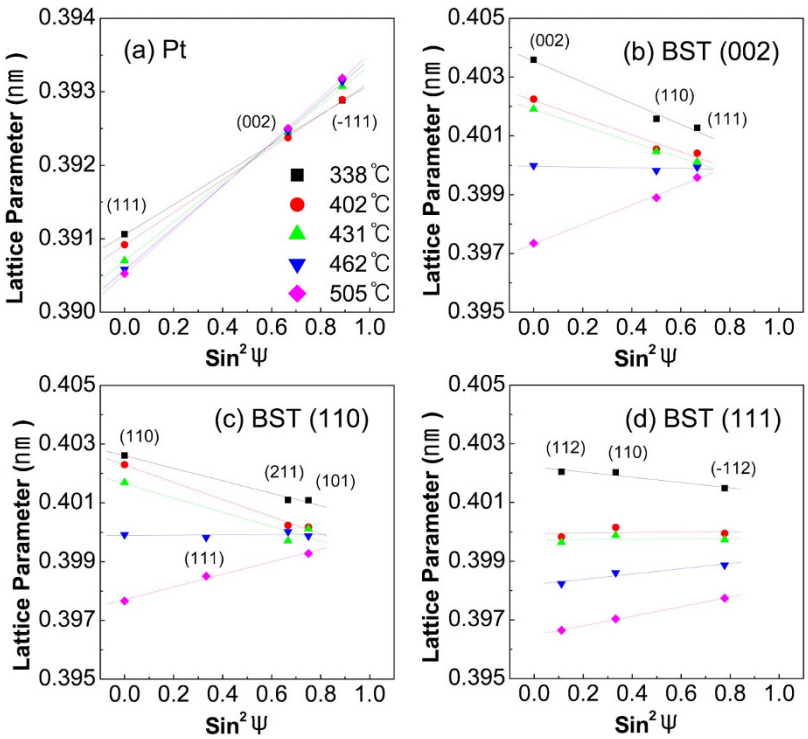

Figure 1 | Variations in the lattice parameters of (a) the Pt electrode film, (b) [002]-, (c) [110]-, and (d) [111]-oriented BST grains as a function of $\sin^2\psi$ for the BST films grown at different T_s.

fitting to $\sin^2\psi = 1$ and 0, ε_0 and ε_z can be estimated for each sample. There are several notable findings from the data sets shown in Fig.1 which could be more evidently seen in Fig. 2.

Figures 2a-d show the variations in the ε_0 and ε_z values as well as the variation of the effective Poisson's ratio, ν ($=-\varepsilon_z/\varepsilon_0$), of the Pt film and those of the three differently oriented BST grains as a function of T_s. In this paper, the positive and negative strains denote the tensile and compressive strains, respectively. The Pt film has only [111]-oriented grains and shows in-plane positive strain at all T_s due to the thermal expansion mismatch with Si (thermal expansion coefficient of Pt $\sim$ 9.6 x 10^{-6} $^{\circ}C^{-1}$)[24]. However, the BST films show complicated development of strains depending on the T_s and types of grains. The [002]- and [110]-oriented grains grown at 505°C show in-plane positive strain, but the same type of grains grown at lower T_s show in-plain negative strains. The cross-over from the positive to negative strain occurs at $\sim$ 460°C. After the abrupt change in the strain state near the transition temperature, the negative strain further develops rather slowly with the decreasing T_s for the [002]-oriented grains. However, that of [110]-oriented grains are rather complicated, which is not yet clearly understood. In addition, the magnitudes of ε_0 and ε_z are symmetric and generally high in [002]-oriented grains due to the higher compliance (S_{11}) and high ν along [002] direction[25,26]. Nevertheless, they are rather asymmetric in [110]-oriented grains along the tensile and compressive directions probably due to the different crystallographic structures. [111]-oriented grains also show in-plane positive strain at the highest T_s but with a smaller magnitude of in- and out-of-plane strains. Interestingly, the transition into the negative strain state occurs at much lower T_s ($\sim$ 400°C). Therefore, the [111]-oriented grains demonstrate an in-plane negative strain state only at the lowest T_s with a much smaller magnitude of ε_0 and ε_z. For this case, the magnitude of ε_z is generally smaller than that of ε_0. The variations in ν appears to be related with the strain state in Figs. 2 (b) and (c), but it is not the case in Fig. 2 (d). Such variations in ν are actually related with the change in Ba/Sr ratio with the varying T_s, and the relative comparison with the theoretically calculated values for the given Ba/Sr ratio has a higher significance as discussed below.

The in-plane tensile stress (positive strain) in BST grains can be generally understood from the thermal expansion mismatch between the film and Si substrate. The influence of Pt and SiO_2 films is negligible due to their much thinner thickness ($\sim$ 0.1 μm) compared to that of Si substrate ($\sim$ 600 μm). The higher in-plane tensile stress state at higher T_s can be understood from the thermal effect. The in-plane compressive stress (negative strain) in sputtered films could be understood from the shot-peening effect[15]. The energetic bombardment of the sputtered particles (especially negatively charged oxygen ions) onto the growing film surface imparts the in-plane compressive stress[15]. Therefore, the increasing in-plane negative strain with the decreasing T_s can be understood from the domination of the ion bombardment effect of the sputtering process over the thermal expansion mismatch. Given the low compliance along the [111] direction of the perovskite BST material[25,26], the out-of-plane strain (ε_z) of the [111]-oriented grains must be smallest at the lowest T_s (338°C), which is indeed the case as shown in Fig. 2d. The same argument can be applied to the in-plane tensile cases; out-of-plane negative strain along the [111] direction is quite small at 505°C, due to the lower in-plane tensile strain at the same temperature compared to the other types of grains. In addition, the lower evolution of compressive stress by the larger decrement of the shot-peening effect in [111]-oriented grains compared to the grains with different orientations decreases the transition temperature from $\sim$ 460 to $\sim$ 400°C. In other words, the thermal effect dominates the mechanical bombardment effect even at lower T_s in [111]-oriented grains. These results must be a natural consequence of the crystallographic-direction specific mechanical properties of the BST material; lower and higher compliance along the [111] and [002] orientations, respectively (See *on-line supplementary information* for the calculation along different directions, and the text below for more discussions. The calculated values are included in Table I.).

In order to confirm whether the different responses of each type of grain to the external stress coincides with the bulk properties of the material, ν under biaxial stress was calculated for the different orientations of the crystals where in-plane biaxial stress (σ_0) was applied to the isolated [111], [110], and [002]-oriented gains, respectively, and the results are compared with the experimental results. These calculations were based on the elastic theory of cubic crystal and compliance tensors of the material with the same cation composition[5,25,26]. It has to be noted that each type of grain must have a completely random in-plane orientation for this comparison to hold its validity, which was indeed the case for [111]- and [002]-type grains but not for [110]-type grains (See Fig. 3), because the film is of the polycrystalline nature. Table I shows the variations in the calculated compliance (ε_0/σ_0 and ε_z/σ_0), and the ν of the crystal with the [111], [110], and [002] directions normal to the stress plane, as well

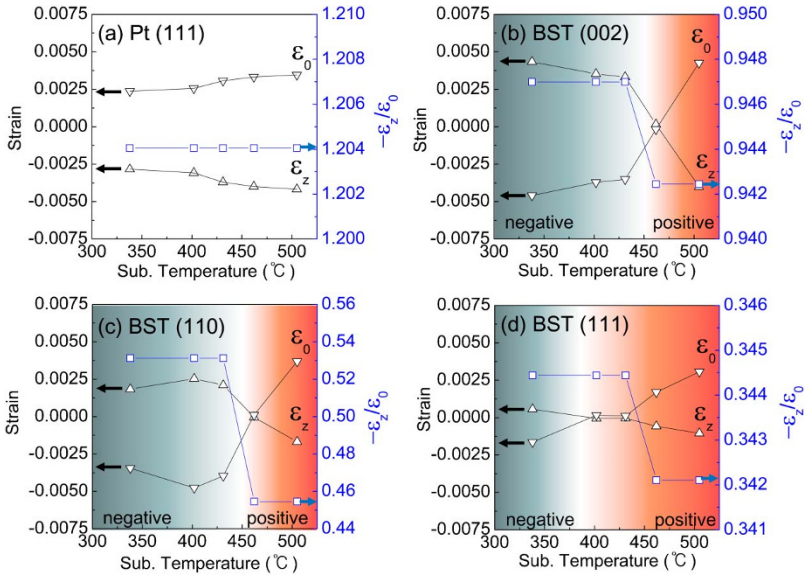

Figure 2 | Variation of in-plane and out-of plane strain as a function of substrate temperature of (a) [111]-oriented grain of Pt, and those of (b) [002]-, (c) [110]-, and (d) [111]-oriented grains of the (Ba,Sr)TiO_3 thin films.

Table I | Comparison between the calculated and experimental Poisson's ratio for 120-nm-thick (Ba,Sr)TiO_3 films with Ba/Sr ratio of 48/52 and 47/53, respectively

Ba/Sr = 48/52						
	ε_0/σ_0	ε_z/σ_0	$-\varepsilon_z/\varepsilon_0$			
	Calc. (10^{-12} m^2/N)		Calc.	Meas. (at 338°C)	Meas. (at 402°C)	Meas. (at 431°C)
[002]	4.076	−3.476	0.853	0.947	0.947	0.947
[110]	3.254	−1.832	0.563	0.531	0.531	0.531
[111]	2.980	−1.284	0.431	0.344	0.344	0.344
Ba/Sr = 47/53						
	ε_0/σ_0	ε_z/σ_0	$-\varepsilon_z/\varepsilon_0$			
	Calc. (10^{-12} m^2/N)		Calc.	Meas. (at 462°C)	Meas. (at 505°C)	
[002]	4.047	−3.439	0.850	0.942	0.942	
[110]	3.240	−1.824	0.563	0.454	0.454	
[111]	2.971	−1.286	0.433	0.342	0.342	

as the ν measured experimentally for the three different types of grain of the BST films grown at the various T_s. Due to the slightly different compositions of the different samples, Ba/Sr ratio of the films grown at 338, 402 and 431°C was taken as 48/52, and that of the other two samples was taken as 47/53.

It is notable that the measured ν of each type of grains is completely independent of T_s for the given Ba/Sr ratio, suggesting the identical mechanical responses of the different grains irrespective of the crystalline quality of the polycrystalline BST films. For the [002]-oriented grains, the measured ν's are generally larger than the theoretically calculated values, suggesting that these grains have higher strains than the theoretically expected values along the out-of-plane direction. In contrast, the measured ν of the [110]- and [111]-oriented grains is smaller than the theoretical value, suggesting that these grains strain less along the out-of-plane direction. In fact, there are several data sets on the value of compliances of $BaTiO_3$ and $SrTiO_3$, from which the compliance values of 48/52 and 47/53 materials are calculated (see table S III of *on-line supplementary information*). Therefore, the theoretical ν's are certainly with some degree of uncertainty. However, the relative comparison between the measured and calculated values is certainly correct. Such a discrepancy between the theoretical and measured values of the ν's and different relative tendency suggest the following. The differently oriented grains experience a significant mechanical confinement effect due

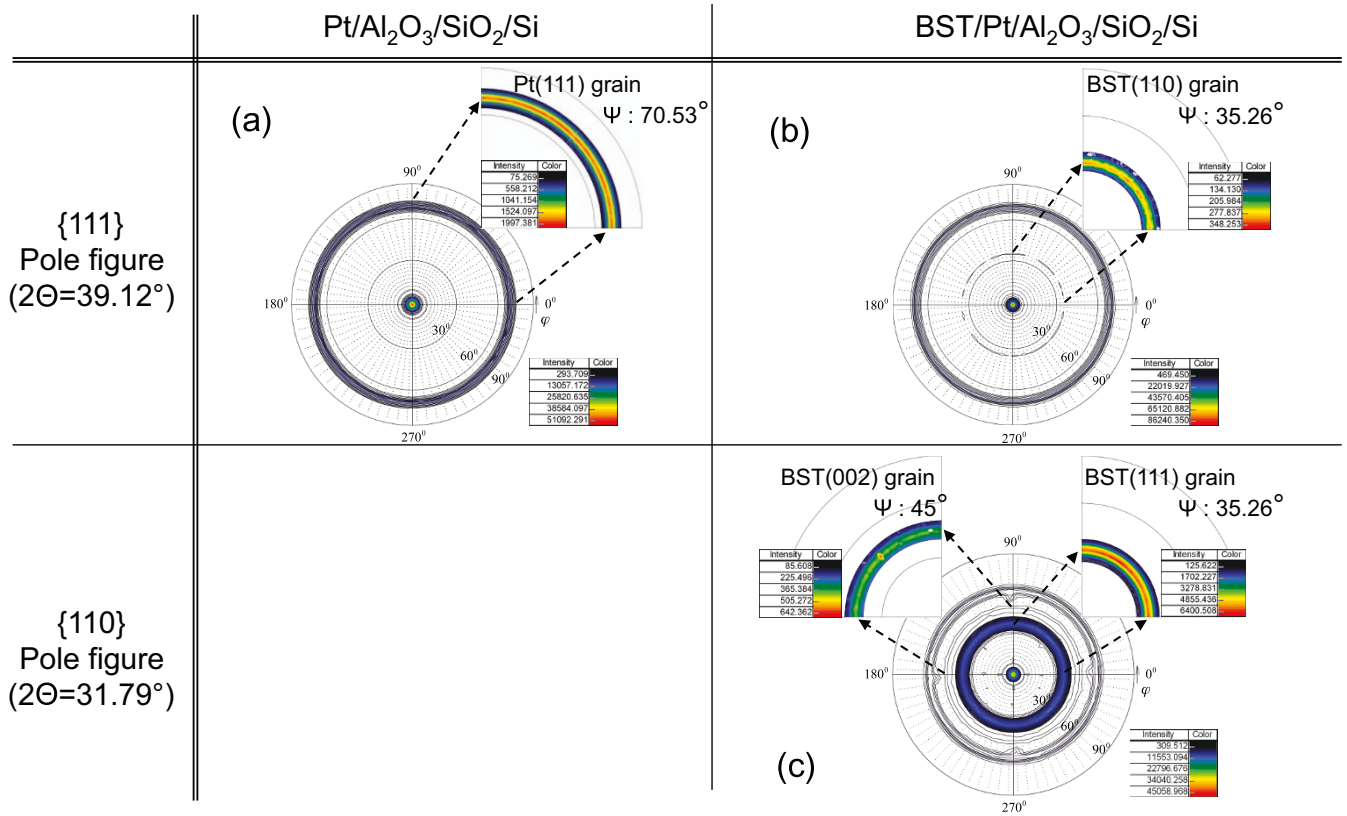

Figure 3 | (a) {111} pole figure of Pt substrate, and (b) {111} pole figure, and (c) {110} pole figure of (Ba,Sr)TiO_3 thin films.

to the densely packed columnar microstructure (see fig. S2 of *on-line supplementary information* for cross-section transmission electron microscopy image) and smaller strain of the [110]- and [111]-oriented grains to the external biaxial stress is compensated by the larger strain of the [002]-oriented grains.

Figure 3 shows the pole figures of [111]-oriented Pt electrode grains (3a, where in-plane distribution of (11-1) type plane is shown), [110]-oriented BST grains (3b, where in-plane distribution of (111) type plane is shown), and [111]- and [002]-oriented BST grains (3c, where in-plane distribution of (110) type plane is shown). The randomness of the in-plane distribution for Pt grains is almost perfect as can be understood from the almost constant distribution of the (11-1) X-ray diffraction peak intensity along the ϕ angle. This was also the case for the [111]- and [002]-oriented grains so that the (110) X-ray diffraction peak intensities along the ϕ angle are almost constant. However, the [110]-oriented grains have a much more non-random in-plane orientation compared to the other cases. Although the exact reason for such an extraordinary behavior is not clearly understood, it might be related with the highly anisotropic nature along the crystallographic directions on the (110) plane compared to the more isotropic nature of the (111) and (002) planes. This may explain the peculiar variations in ε_z and ε_0 of this type of grain shown in Fig. 2c. However, it appears that such a discrepancy in the degree of randomness of the in-plane orientation does not influence the mechanical confinement effect largely.

The different mechanical responses of the different types of grains, shown in Fig. 2, can be understood from the calculated compliance values and Poisson's ratio along the different directions of the bulk crystal shown in table I. The absolute value of the out-of-plane compliance along the [111] is the smallest and that along the [002] is the largest. The possible reasons for such a discrepancy was considered from the possible distortion of the TiO_6 octahedra, which are the building blocks of the BST material in response to the external stress, and the results are included in the Fig. S3 of *on-line supporting information*. Due to the different compliance values along the different crystallographic directions, the different types of grains response differently to the mechanical stress along the in-plane direction; under the given (in-plane) compressive stress, for example, the smaller compliance of the [111]-oriented grains results in the smaller elongation along the out-of-plane direction than the theoretical value because the other type of grains elongate more than the theoretical value due to their higher compliance along those directions.

Next, the defect (mainly oxygen vacancy) concentrations of each type of grain are considered. Various thin films processing techniques of oxide films usually induce oxygen vacancy generation for various reasons. In the sputtering process of BST films, the low oxygen partial pressure and shot-peening effect generally induce high oxygen vacancy concentration[15,27,28]. The average oxygen vacancy concentration, therefore, must be specifically determined by the adopted process conditions. However, due to the oxygen vacancy being generally low in density, it is often difficult to measure them by available spectroscopic means. In addition, it has not been feasible to estimate the oxygen vacancy concentrations in each type of grain within poly-crystalline oxide films. However, the accurate determination of the lattice parameters for each type of grain makes this possible as shown below. This is based on the work by Kim et al. where the lattice parameters of oxygen-deficient bulk BST material is reported to be determined by the oxygen vacancy concentration, which was controlled by the equilibrium oxygen partial pressure during annealing, for the given cation composition[29]. One possible problem in applying the same method to the thin films, as in this work, is to achieve an unstrained lattice parameter (a_0) for the differently oriented grains, which are free from the influence of any strain. This becomes possible by adopting the $\sin^2\psi$ method again. Details for the determination of a_0 using the $\sin^2\psi$ method were also, and the calculated $\sin^2\psi$ values for each type of grain for the cases of Ba/Sr ratios of 48/52 and 47/53 are included in the table S IV of *on-line supporting information*.

Figure 4 shows the variation in the measured a_0 of the differently oriented BST grains as well as the Pt as a function of T_s. There are three notable findings; first, they are generally much larger than the bulk lattice parameter with the same cation composition (a_0 of bulk $Ba_{0.5}Sr_{0.5}TiO_3$ is 0.3947 nm, being indicated by a dashed line in Fig. 4). Second, the a_0 for each type of grain generally decreases with the increasing T_s having a different decreasing rate. Third, the a_0 for each type of grain are not the same. At $T_s = 338^\circ C$ the difference is quite small. The largest a_0 was achieved from the [111]-oriented grains but the difference with a_0 of [002]-oriented grains, which is the smallest, is only ~ 0.002 nm. (See Table S V of *on-line supporting information* for the detailed numbers of a_0) As T_s increases, the a_0 of the [111]-oriented grains decreases more significantly than the others and it becomes the smallest when T_s is $> 400^\circ C$. In addition, the difference with the other types of grains becomes larger as T_s increases. At $T_s = 402^\circ C$, the a_0 of [110]-oriented grains is the largest but that of [002]-oriented grains becomes the largest at $505^\circ C$. Overall, the difference between the [002]- and [110]-oriented grains are generally smaller than that with [111]-oriented grains. It needs to be stressed that these lattice parameters are not influenced by the in- and out-of-plane strains.

The larger a_0 values for the various types of grains in BST thin film correspond to the higher oxygen vacancy concentration[29]. The estimated identical a_0 of the Pt electrode to that of the bulk Pt material (down triangle symbol in Fig. 4) irrespective of the processing conditions suggests that other effects, such as strain and sputtering damage, can hardly influence the unstrained lattice parameters of the materials in the system. The different a_0 values of the BST grains with different orientations suggest that the oxygen vacancy concentration is also different. According to the results given by Kim et al. the oxygen vacancy concentration for the lattice parameters of 0.4020 nm is three times larger than that of 0.3970 nm. (It must be noted that the absolute values of the oxygen vacancy concentration cannot be compared but only relative values can be estimated in this way.) In other words, the different oxygen vacancy concentrations in different types of grains results in the different a_0 values even when all the grains were formed simultaneously under the given sputtering conditions. In general, the larger a_0 values compared to the bulk value of all cases suggest that all the films are generally oxygen deficient by the knock out effect from the energetic particle bombardments during the sputtering.

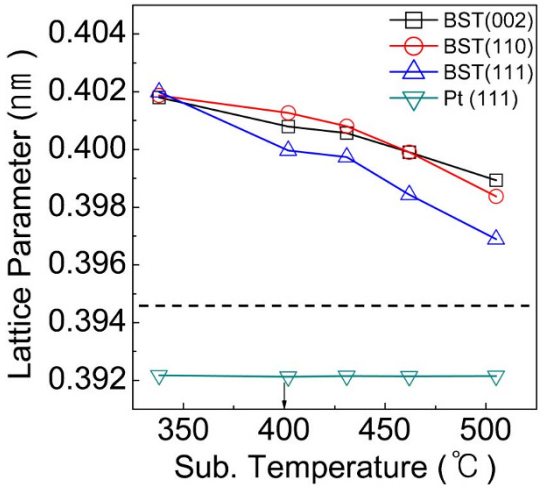

Figure 4 | Variation in the measured unstrained lattice parameter, a_0, of the differently oriented $(Ba,Sr)TiO_3$ grains as well as the Pt as a function of substrate temperature. Dashed line indicates the bulk value of $(Ba,Sr)TiO_3$.

The different variations in a_0 for the three types of grains with increasing T_s are understood as follows. The almost identical a_0 at the T_s of 338°C suggests that the vacancy concentration is dominantly determined by the knocking out effect during the sputtering process, which must be identical for all the three types of grains. The surface of the BST film was quite smooth demonstrating a highly uniform grain size irrespective of the types of grain due to the relatively incomplete crystallization at this low T_s (See Fig. S 2b of *on-line supporting information*). It can be also understood that the in-plane compressive stress does not influence the vacancy concentration since the three types of grains have different levels of strains (Fig. 2). As the T_s increases, the thermal healing effect appears to work and the vacancy concentration generally decreases. The larger decrease in the vacancy concentration for the [111]-oriented grains compared to the other two cases cannot be explained by the in-plane tensile stress effect, although this can be thought to be the case because the transition into the in-plane tensile stress state already occurs at ~ 400°C for this case while the other two types of grains still remain in the in-plane compressive state up to ~ 460°C. This can be understood from the fact that the positive strain of the [111]-oriented grains is the lowest among the three but the vacancy concentration was the lowest (smallest a_0) for this case at the T_s of 505°C. In fact, given the finding that the negative in-plane strain does not invoke any difference in the vacancy concentration between the different types of grains (338°C), it may not be reasonable to consider that the tensile stress induces the difference. Therefore, there must be some other factors, which influence the degree of oxygen vacancy healing depending on the types of grains.

It has been reported that the in-situ well-crystallized polycrystalline $SrTiO_3$, $BaTiO_3$ (BTO), and BST films tend to have roughened surface morphology due to the different growth habit planes of each grain[30]. Hwang *et al.* reported that the [111]-oriented grains of BTO on the highly [111]-oriented Pt thin film electrode grows only on the vicinal planes of the [111]-oriented Pt grains while the [002]- and [110]-oriented grains grow on the (111) plane of the Pt grains[31]. They invoked different surface charges and surface energies of the BTO materials depending on the types of crystallographic surfaces for such peculiar behavior of (local) epitaxial growth for such ionic oxide (BTO) on the metal (Pt) surface although the lattice mismatch is generally favorable for the usual epitaxial growth. Furthermore, the emergence of the three types of grains in this work is also believed to be due to such surface and interface-charge related arguments. As a result, the [002]- and [110]-oriented BST grains tend to have a flat surface as they may grow on the flat surface region of the [111]-oriented Pt grains, while the [111]-oriented BST grains tend to grow on the vicinal area of the Pt grains, which eventually results in the larger specific surface area of the [111]-oriented grains compared to the other two types of grain. (See Fig. S2 of *on-line supporting information* for TEM and atomic force microscopy (AFM)) Although this cannot be directly confirmed due to the lack of crystallographic information in the AFM images, the relatively rough surface morphology of the Pt electrode and several protruded grain shapes of BST films revealed by AFM (Fig. S2 of *on-line supporting information*) revealed that the specific surface area of the [111]-oriented BST grains is larger than those of the two others. TEM also confirmed this (See Fig. S2 of *on-line supporting information*). The larger surface energy of (111) planes also contribute to the suppression of the flat (111) surface in [111]-oriented BST grains. With this assumption, the faster healing effect of the [111]-oriented grains can be understood; the larger surface area of this type of grain enhances the vacancy annihilation during the growth at a higher T_s. At lower T_s, the generally less evident evolution of grain morphology of the different grains makes this difference less evident and thus the vacancy healing effect must be averaged out.

Up to now, the influences of T_s on the evolution of strain and oxygen vacancy concentration for each type of BST grains have been discussed. Next, the effects of film thickness (t_f) on the evolution of the strains will be discussed for the films grown at 505°C. t_f was varied from 29.6 nm to 155.8 nm, and the detailed information of these films, such as the Θ-2Θ XRD data and cation composition are included in the *on-line supporting information* (Figures S4 and S5). All the films showed identical crystallographic growth behavior and cation compositions irrespective of the t_f within the experimental error (< ~ 1 at. %).

The in- and out-of-plane strains of the [111]-, [110]- and [002]-oriented grains are also examined by the $\sin^2\psi$ method, and the variations in the lattice parameters of Pt electrode film, [111]-, [110]-, and [002]-oriented BST grains, respectively, as a function of $\sin^2\psi$ for the BST films with different t_f are included in Fig. S6 of *on-line supporting information*. The results for the BST grains are summarized in Fig. 5. Figures 5a-c show the variations in the ε_0 and ε_z values as a function of the t_f for the three differently oriented grains. The ε_0 and ε_z values generally decrease with the increasing t_f. However, the overall difference between the different types of grains is quite identical to that shown in Fig. 2; the strain of [002]-oriented grains is symmetrical and largest while that of [111]-oriented grains is asymmetrical and smallest. Table II shows the same comparison between the calculated and measured ν values of the three types of grains at two representative t_f. The experimental ν of the other t_f films are exactly the same as those shown in table II. A same tendency as that in table I can be found.

Figure 5d shows the variations of unstrained lattice parameter (a_0) for the different types of grains as a function of t_f. Bulk a_0 value (0.3947 nm) of the $(Ba_{0.5},Sr_{0.5})TiO_3$ is indicated by dashed line in the figure. The a_0 for each type of grain is almost independent of the t_f but only depends on the type of the grain. This means that the overall oxygen vacancy concentration is not dependent on t_f while the strain is dependent on it. Moreover, this suggests that the strain relaxations shown in Fig. 5a-c are not due to healing out of the oxygen vacancies or agglomeration of the oxygen vacancies to form the dislocations. Conversely, this also coincides with the fact that the film stress hardly has an influence on the vacancy concentration, as discussed above.

Discussion

In this work, the strain state of in-situ crystallized poly-crystalline BST thin films on Pt electrodes was carefully examined using the $\sin^2\psi$ method in the X-ray diffraction technique. The poly-crystalline BST thin films deposited at substrate temperatures ranging from 338 to 505°C showed a relatively random orientation with [002]-, [110]-, and [111]-oriented grains along the normal direction to the surface, of which strain states are different although they were grown simultaneously. In addition, the transition temperature where the strain state of each grain changes from the in-plane compressive state, which is believed to be due to the shot-peening effect of the sputtering process, to the in-plane tensile state, which is due to the thermal expansion mismatch between the BST film and substrate, was also different. This is a highly unexpected result as opposed to the general conjecture that the every grain in poly-crystalline film has an identical strain (and stress, too) under the given growth conditions due to the strong mechanical confinement between the neighboring grains. The different compliances along the out-of-plane direction of the different types of grains resulted in the different strains responding to the external in-plane stress.

The unstrained lattice parameter, which is dominantly governed by the oxygen vacancy concentration for each type of grain, was also different suggesting the vacancy concentration is different. Interestingly, such a discrepancy has no correlation with the different strain state for each type of grain but appeared to be related with the specific surface area, which provides the grains with oxygen atoms at higher growth temperatures.

The trends of the orientation-specific strain state was maintained in a wide thickness range (29.6 ~ 155.8 nm) although thicker films

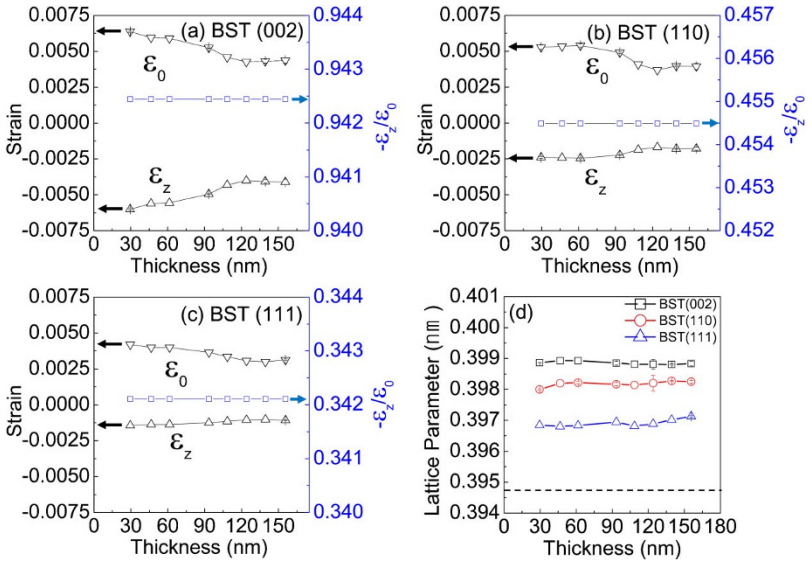

Figure 5 | Variation of in-plane and out-of plane strain as a function of film thickness for the cases of (a) [002]-, (b) [110]-, and (c) [111]-oriented grains of the (Ba,Sr)TiO_3 thin films, and (d) comparison of lattice parameter (Ba,Sr)TiO_3 grains with different orientations. Dashed line indicates the bulk value of (Ba,Sr)TiO_3.

generally show decreased strains perhaps due to the generation of misfit dislocations. However, the orientation-specific unstrained lattice parameter was constantly maintained suggesting that the different vacancy concentration for each type of grain is independent of the film thickness.

Perhaps the most striking feature that this work figured out from the detailed X-ray study on such an ionic crystalline material is different oxygen vacancy concentration in each type of grains. Even further unexpected finding is that the oxygen vacancy concentration has nothing to do with the strain state of each grain.

It is believed that this work may invoke a new aspect of mechanical and chemical nature regarding poly-crystalline thin films. However, it must be noted that there could be many other thin film systems that show different levels of mechanical interactions between the grains (perhaps metals or covalently bonded materials have different tendency), which could be checked by the same X-ray technique. It is hoped that this technique can be more widely applied to many other poly-crystalline material systems in order to elucidate their mechanical and chemical nature of different grains.

Methods

After the Si substrate was cleaned, 100-nm-thick SiO_2 was thermally grown and 10-nm-thick amorphous Al_2O_3 layer was deposited by an atomic-layer-deposition process in order to improve the adhesion between the substrate and the Pt electrode that was deposited on top by a dc sputtering technique. The Pt electrode thickness was 100 nm and had a highly [111] preferred growth behavior in the out-of-plane direction while the crystallographic direction in the in-plane direction is completely random. BST films with thicknesses ranging from 29.6 to 155.8 nm were deposited by an rf sputtering technique using a ceramic target under a sputtering pressure of 10 mTorr (O_2/Ar gas ratio = 10%). The substrate temperature was varied from 338 to 505°C. 338°C was just enough T_s to grow the *in-situ* crystallized poly-crystalline BST film. Film cation composition ratios, [Ti]/[Ba+Sr+Ti] and [Ba]/[Ba+Sr], were estimated by X-ray fluorescence spectroscopy (See *on-line supporting information*).

X-ray diffraction was performed using a Cu *kα* radiation, which was monochromatized by a curved graphite monochromator. A Hybrid Mirror type X-ray detector was used to enhance the resolution and minimize the measurement error and analysis time. The Θ-2Θ scan was used to determine the crystallographic orientation of the film. The $\sin^2\psi$ method was used in order to detect the strain and unstrained lattice parameter of each grain. Lastly, the X-ray pole figure measurement was also used to determine the degree of randomness of the in-plane crystallographic direction for each type of grain.

The microstructure of the film was observed using high-resolution transmission electron microscopy (HRTEM) and atomic force microscopy (AFM) (See *on-line supporting information*).

Table II | Comparison between the calculated and experimental Poisson's ratio for the cases of 29.6-nm- and 155.8-nm-thick (Ba,Sr)TiO_3 films grown at 505°C

	ε_0/σ_0	ε_z/σ_0	$-\varepsilon_z/\varepsilon_0$		
	Calc. (10^{-12} m^2/N)		Calc.	Meas. (at 29.6 nm)	Meas. (155.8 nm)
[002]	4.047	−3.439	0.850	0.942	0.942
[110]	3.240	−1.824	0.563	0.454	0.454
[111]	2.971	−1.286	0.433	0.342	0.342

1. Choi, K. J. *et al.* Enhancement of Ferroelectricity in Strained $BaTiO_3$ Thin Films. *Science* **306**, 1005–1009 (2004).
2. Lee, H. N., Hesse, D., Zakharov, N. & Gösele, U. Ferroelectric $Bi_{3.25}La_{0.75}Ti_3O_{12}$ Films of Uniform a-Axis Orientation on Silicon Substrates. *Science* **296**, 2006–2009 (2002).
3. Wang, J. *et al.* Epitaxial $BiFeO_3$ Multiferroic Thin Film Heterostructures. *Science* **299**, 1719–1722 (2003).
4. Neaton, J. B. & Rabe, K. M. Theory of polarization enhancement in epitaxial $BaTiO_3$/$SrTiO_3$ superlattices. *Appl. Phys. Lett.* **82**, 1586–1588 (2003).
5. Pertsev, N. A., Zembilgotov, A. G. & Tagantsev, A. K. Effect of Mechanical Boundary Conditions on Phase Diagrams of Epitaxial Ferroelectric Thin Films. *Phys. Rev. Lett.* **80**, 1988–1991 (1998).
6. Uwe, H. & Sakudo, T. Stress-induced ferroelectricity and soft phonon modes in $SrTiO_3$. *Phys. Rev. B* **13**, 271–286 (1976).
7. Pertsev, N. A., Kukhar, V. G., Kohlstedt, H. & Waser, R. Phase diagrams and physical properties of single-domain epitaxial $Pb(Zr_{1-x}Ti_x)O_3$ thin films. *Phys. Rev. B* **67**, 054107 (2003).
8. Ban, Z.-G. & Alpay, S. P. Optimization of the tunability of barium strontium titanate films via epitaxial stresses. *J. Appl. Phys.* **93**, 504–511 (2003).
9. Chang, W., Gilmore, C. M. & Kim, W.-J. Influence of strain on microwave dielectric properties of (Ba,Sr)TiO_3 thin films. *J. Appl. Phys.* **87**, 3044–3049 (2000).
10. Pertsev, N. A., Zembilgotov, A. G., Hoffmann, S., Waser, R. & Tagantsev, A. K. Ferroelectric thin films grown on tensile substrates: Renormalization of the Curie–Weiss law and apparent absence of ferroelectricity. *J. Appl. Phys.* **85**, 1698–1701 (1999).
11. Yuzyuk, Y. I., Simon, P., Zakharchenko, I. N., Alyoshin, V. A. & Sviridov, E. V. Stress effect on the ferroelectric-to-paraelectric phase transition in heteroepitaxial (Ba,Sr)TiO_3/(001)MgO thin film studied by Raman scattering and x-ray diffraction. *Phys. Rev. B* **66**, 052103 (2002).
12. Lee, B., Lee, C. K., Han, S., Lee, J. & Hwang, C. S. First-principles calculation of capacitance including interfacial effects. *J. Appl. Phys.* **103**, 024106 (2008).
13. Stengel, M. & Spaldin, N. A. Origin of the dielectric dead layer in nanoscale capacitors. *Nature* **443**, 679–682 (2006).

14. Stengel, M., Vanderbilt, D. & Spaldin, N. A. Enhancement of ferroelectricity at metal–oxide interfaces. *Nature Mater.* **8**, 392–397 (2009).
15. Park, W. Y., Ahn, K. H. & Hwang, C. S. Effects of in-plane compressive stress on electrical properties of (Ba,Sr)TiO_3 thin film capacitors prepared by on- and off-axis rf magnetron sputtering. *Appl. Phys. Lett.* **83**, 4387–4389 (2003).
16. Haeni, J. H. *et al.* Room-temperature ferroelectricity in strained $SrTiO_3$. *Nature* **430**, 758–761 (2004).
17. Lee, H. N., Christen, H. M., Chisholm, M. F., Rouleau, C. M. & Lowndes, D. H. Strong polarization enhancement in asymmetric three-component ferroelectric superlattices. *Nature* **433**, 395–399 (2005).
18. Kim, Y. S. *et al.* Observation of room-temperature ferroelectricity in tetragonal strontium titanate thin films on $SrTiO_3$ (001) substrates. *Appl. Phys. Lett.* **91**, 042908 (2007).
19. Ramesh, R. & Schlom, D. G. Orienting Ferroelectric Films. *Science* **296**, 1975–1976 (2002).
20. Park, W. Y. *et al.* Unusual thickness dependence of permittivity and elastic strain in Sc modified epitaxial (Ba,Sr)TiO_3 thin films. *Appl. Phys. Lett.* **92**, 102902 (2008).
21. Jun, S., Kim, Y. S., Lee, J. & Kim, Y. W. Dielectric properties of strained (Ba, Sr)TiO_3 thin films epitaxially grown on Si with thin yttria-stabilized zirconia buffer layer. *Appl. Phys. Lett.* **78**, 2542–2544 (2001).
22. Ban, Z.-G. & Alpay, S. P. Phase diagrams and dielectric response of epitaxial barium strontium titanate films: A theoretical analysis. *J. Appl. Phys.* **91**, 9288–9296 (2002).
23. Noyan, I. C. & Cohen, J. B. *Residual Stress: Measurement by Diffraction and Interpretation*, Springer-Verlag, New York (1987).
24. Zhou, J. *et al.* Bridgman growth and characterization of nonlinear optical single crystals $Ca_4GdO(BO_3)_3$. *Mat. Sci. Eng. B* **97**, 283–287 (2003).
25. Nix, W. D. Mechanical-properties of thin-films *Metall. Trans.* **20A**, 2217–2245 (1989).
26. Nye, J. F. *Physical Properties of Crystals*, Oxford University Press, London (1957).
27. Shin, J. C., Park, J., Hwang, C. S. & Kim, H. J. Dielectric and electrical properties of sputter grown (Ba,Sr)TiO_3 thin films. *J. Appl. Phys.* **86**, 506–513 (1999).
28. Baniecki, J. D., Shioga, T., Kurihara, K. & Kamehara, N. Investigation of the importance of interface and bulk limited transport mechanisms on the leakage current of high dielectric constant thin film capacitors. *J. Appl. Phys.* **94**, 6741–6748 (2003).
29. Kim, W. J., Chang, W., Qudri, S. B., Pond, J. M., Kirchoefer, S. W., Chrisey, D. B. & Horwitz, J. S. Mocrowave properties of tetragonally distorted (Ba0.5Sr0.5)TiO3 thin films. *Appl. Phys. Lett.* **76**, 1185–1187 (2000).
30. Hwang, C. S. *et al.* Deposition and electrical characterization of very thin $SrTiO_3$ films for ultra large scale integrated dynamic random access memory application. *Jpn. J. Appl. Phys.* **34**, 5178–5183 (2005).
31. Hwang, C. S., Vaudin, M. D. & Schenk, P. K. Influence of the microstructure of Pt/Si substrates on textured growth of barium titanate thin films prepared by pulsed laser deposition. *J. Mater. Res.* **13**, 368–375 (1998).

Acknowledgments

This work was supported by the Converging Research Center Program (2012K001299), and the Global Research Laboratory program (2012040157) through the National Research Foundation (NRF) of Korea.

Author contributions

W.Y.P. performed the deposition and X-ray experiments, and analyzed the data; M.H.P. analyzed HRTEM and AFM images, and wrote the paper partly; J.H.L. performed HRTEM analysis; J.H.Y. performed AFM analysis.; J.H.H. wrote the paper partly; J.H.C. and C.S.H. designed the experiments, and wrote the paper.

Additional information

Supplementary information accompanies this paper at http://www.nature.com/scientificreports

Competing financial interests: The authors declare no competing financial interests.

License: This work is licensed under a Creative Commons Attribution-NonCommercial-NoDerivs 3.0 Unported License. To view a copy of this license, visit http://creativecommons.org/licenses/by-nc-nd/3.0/

How to cite this article: Park, W.Y. *et al.* Strain evolution of each type of grains in poly-crystalline (Ba,Sr)TiO_3 thin films grown by sputtering. *Sci. Rep.* **2**, 939; DOI:10.1038/srep00939 (2012).